Hydrogen terminated 4H-SiC($1\bar{1}00$) and ($11\bar{2}0$) surfaces studied by synchrotron x-ray photoelectron spectroscopy

Th. Seyller,[1,*] R. Graupner,[1] N. Sieber,[1] K. V. Emtsev,[1] L. Ley,[1] A. Tadich,[2] J. D. Riley,[2] and R. C. G. Leckey[2]
[1]*Institut für Technische Physik, Lehrstuhl für Experimentalphysik, Universität Erlangen-Nürnberg, Erwin-Rommel-Str.1, 91058 Erlangen, Germany*[†]
[2]*Department of Physics, La Trobe University, Bundoora, Victoria 3083, Australia*
(Received 13 July 2004; revised manuscript received 8 March 2005; published 30 June 2005)

Using x-ray photoelectron spectroscopy (XPS), synchrotron x-ray photoelectron spectroscopy (SXPS), low-energy electron diffraction (LEED), and Fourier- transform infrared absorption spectroscopy (FTIR) we have investigated structure and composition of hydrogen saturated 4*H*-SiC($1\bar{1}00$) and ($11\bar{2}0$) surfaces. The hydrogen saturated surfaces are clean and unreconstructed. On both surface orientations a hydrogen induced surface core level shift is observed in the C 1*s* spectra, which is consistent with carbon monohydrides. The identification of a corresponding component in the Si 2*p* spectra is discussed. On 4*H*-SiC($1\bar{1}00$) a sharp absorption line due to the Si-H stretch mode indicates the presence of silicon monohydrides. Structural models for hydrogen saturated 4*H*-SiC($1\bar{1}00$) and ($11\bar{2}0$) surfaces are proposed which are consistent with our spectroscopic results. Annealing in ultrahigh vacuum leads to considerable changes in the core level spectra although the surface periodicity remains unchanged at (1×1). The thermally induced line shape variations are more prominent in the C 1*s* spectra than in the Si 2*p* spectra.

DOI: 10.1103/PhysRevB.71.245333 PACS number(s): 68.35.Bs, 68.43.Fg, 68.43.Jk

I. INTRODUCTION

Silicon carbide (SiC) is a wide band gap semiconductor with properties that make it interesting for power electronic devices. As a consequence, crystal growth and materials properties of SiC have been studied intensively during the last decade.[1] Growth of SiC single crystals is performed using the modified Lely technique on seed crystals with the surface normal parallel to the *c* axis of the hexagonal unit cells of 4*H*- and 6*H*-SiC.[2,3] For example, 4*H*-SiC is grown on the C-terminated ($000\bar{1}$) surface while growth of 6*H*-SiC is carried out on the Si-terminated (0001) surface.[4–6] Since both (0001) and ($000\bar{1}$) surfaces consist of either Si or C atoms only, these surfaces have to be considered as polar surfaces.

As an alternative to growth on the polar {0001} surfaces, the use of seed crystals oriented in ($1\bar{1}00$) or ($11\bar{2}0$) direction has been investigated.[7–9] These nonpolar surfaces, which are frequently referred to as *a* planes, possess a surface normal oriented perpendicular to the *c* axis or in other words, their surface plane is running parallel to the *c* axis. Note that the two surfaces are also perpendicular to each other. A major advantage of these alternative growth directions is that the formation of micro pipes, a hollow core screw dislocation along the *c* axis with inner diameters of up to a few tens of microns, is completely suppressed. Furthermore, the nonpolar ($1\bar{1}00$) and ($11\bar{2}0$) surfaces expose the information about the stacking sequence of the seed crystal, thus acting as a template inhibiting polytype fluctuations. Nevertheless, it was observed that the number of stacking faults is higher in crystals grown on a-planes than in crystals grown in the conventional way by a factor of 10^2–10^3 on ($11\bar{2}0$) and 10^3–10^4 on ($1\bar{1}00$), respectively.[7,8] This observation was explained by a kinetically induced disarrangement of adatoms on the growing surface.[7] Recently, however, Nakamura *et al.*[10] reported the growth of high quality, almost dislocation free 4*H*-SiC by using a so-called repeated *a* face (RAF) growth. In addition to bulk growth, chemical vapor deposition on 4*H*-SiC($11\bar{2}0$) was studied as well[11,12] and extremely flat surfaces without step-bunching and without triangular defects were observed.

Another interesting aspect of the ($11\bar{2}0$) surface of SiC is connected to the quality of the interface between thermally grown SiO_2 and SiC. For MOSFETs on SiC(0001) a low channel mobility is observed due to a large density of electrically active interface states (D_{it}).[13] So far, this prevents SiC from being used in MOSFET devices. The reason for the high D_{it} is twofold.[14] Incomplete oxidation of carbon is supposed to lead to the formation of carbon clusters which are responsible for high D_{it} values near midgap position. In addition, so-called near interface traps exist which are energetically located just below the conduction band minimum of 4*H*- and 6*H*-SiC. Their microscopic origin is still unclear. Different recipes such as nitridiation of the interface[15] or use of alternative gate oxides[16] are currently investigated in order to reduce D_{it}, but it was also shown that by using the 4*H*-SiC($11\bar{2}0$) surface a reduction of D_{it} can be achieved which is accompanied by an increased channel mobility.[13,17,18] The microscopic origin of this different behavior of the Si face and the ($11\bar{2}0$) plane is unclear as yet. However, recent oxidation studies on 4*H*-SiC($11\bar{2}0$) reported the formation of Si in more than two oxidation states[19–21] which is in contrast to the (0001) surface where only Si^+ is observed at the interface to SiO_2.[22–25] In addition, unlike with SiO_2-SiC(0001)[22–24] chemically shifted components were also observed in the C 1*s* core level spectra,[20,21] which may signal the presence of

 ©2005 The American Physical Society

C-O bonds at the interface. These results indicate that the structural elements present in the SiO_2-SiC interface depend strongly on the surface orientation which in turn may lead to a different defect formation mechanism as indicated by the electrical measurements.[21]

Despite these interesting aspects of nonpolar SiC surfaces only little is known about their structural and electronic properties. Until recently, only theoretical studies of nonpolar SiC surfaces have been reported[26–29] and nothing was known about the preparation of clean nonpolar surfaces of 4*H*- and 6*H*-SiC. Using photoelectron spectroscopy, Virojanadara and Johansson[20] have studied the structural and electronic properties of 4*H*-SiC$(1\bar{1}00)$ and $(11\bar{2}0)$ surfaces after wet-chemical treatment and after annealing in UHV at temperatures of up to 1150 °C.[20] The wet-chemically cleaned surfaces contained considerable amounts of oxygen. After desorption of oxygen at approximately 1000 °C the core level spectra taken from the (1×1) surfaces revealed surface related chemically shifted components, which were extremely weak in the Si 2*p* spectra but considerably larger in the C 1*s* spectra. This was taken as evidence that the surface structure is predominantly carbon rich, which is contrary to the silicon rich phases proposed by Rauls *et al.*[28,29] The latter performed self-consistent charge density-functional based tight-binding (SCC-DFTB) calculations to study the clean *a* planes of 2*H*-, 4*H*-, and 6*H*-SiC and found that on both *a* planes Si rich phases are stable even under carbon rich conditions. On the other hand, Si enrichment was observed on 6*H*-SiC$(11\bar{2}0)$ after deposition of Si followed by annealing in ultrahigh vacuum (UHV).[30] In this case, too, a (1×1) periodicity was observed by reflection high-energy electron diffraction. Annealing the 4*H*-SiC$(1\bar{1}00)$ in a flux of silicon leads to the formation of Si-rich $c(4\times2)$ and $c(2\times2)$ reconstructions.[31,32]

One method to prepare clean, polar SiC{0001} surfaces is hydrogenation by annealing in ultra-pure hydrogen at temperatures around 1000 °C. This method was first suggested by Tsuchida and co-workers.[33–36] We have adopted this method and have studied the chemical, structural and electronic properties of hydrogenated 6*H*-SiC{0001} surfaces.[37–45] The surfaces prepared in this way are free of unwanted contaminants, unreconstructed, chemically inert, and—within certain limits—electronically passivated. As will be shown in the present paper, hydrogenation leads to clean and unreconstructed nonpolar surfaces of 4*H*-SiC. Furthermore, by applying our knowledge about the H-terminated, polar {0001} surfaces it is possible to develop structure models for the hydrogen saturated 4*H*-SiC$(1\bar{1}00)$ and $(11\bar{2}0)$ surfaces. Because the hydrogen saturated surfaces are stoichiometric and unreconstructed they are ideal starting points for observing the formation of reconstructions. Therefore, we have annealed the hydrogen terminated surfaces in UHV to a maximum temperature of 990 °C. Our experimental observations are discussed in the light of our earlier studies on the hydrogenated basal planes of 6*H*-SiC[37–45] and of the previous study by Virojanadara and Johansson on wet-chemically prepared a-planes.[20]

The paper is organized as follows. Section II will briefly describe the experimental aspects of the present work. In Sec. III the experimental results will be discussed. As will be shown in Secs. III A and III B the combination of XPS, LEED, and SXPS allows us to propose structural models for the hydrogenated a-planes of 4*H*-SiC which are presented in Sec. III C. The effect of annealing at temperatures of up to 990 °C in UHV on these surfaces is discussed in Sec. III D. Finally, in Sec. IV a brief summary and outlook will be given.

II. EXPERIMENTAL

4*H*-SiC wafers with $(1\bar{1}00)$ and $(11\bar{2}0)$ surface orientation were purchased from Cree Research, Inc. The $(1\bar{1}00)$ samples were exclusively *n* doped but both *p* and *n* type $(11\bar{2}0)$ samples were investigated as reference for further studies. The samples were cleaned by a wet-chemical procedure using hydrofluoric acid and mixtures of sulphuric acid, hydrogen peroxide, hydrochloric acid, and water as described elsewhere.[46,47] Hydrogenation was carried out by annealing the samples in purified hydrogen (grade 8.0) at temperatures around 1000 °C and a pressure of 1 bar. Heating was achieved by a contact-less infrared heating system consisting of five 1000 W halogen lamps. The base pressure of the UHV preparation chamber was around 1×10^{-8} mbar. After preparation the samples were placed in a transportable vacuum storage chamber equipped with a mobile ion pump providing a base pressure below 1×10^{-8} mbar. Using this vacuum transfer we are able to transport up to six hydrogenated samples to the experimental stations in our laboratory or to the synchrotron radiation source BESSY II without exposing the samples to air.

The samples were investigated in our home laboratory by x-ray induced photoelectron spectroscopy (XPS) using monochromatized Al K_α radiation ($\hbar\omega=1486.6$ eV) with an overall resolution of 0.6 eV and low-energy electron diffraction (LEED). In addition, selected samples were also investigated *ex situ* with Fourier-transform infrared absorption spectroscopy in attenuated total reflection mode (FTIR-ATR) using a Ge prism as multiple internal reflection element. Synchrotron x-ray photoelectron spectroscopy (SXPS) was carried out at undulator beamline UE56/2-PGM1 at BESSY II. The end station with a base pressure below 1×10^{-10} mbar mbar was equipped with a hemispherical analyzer and a LEED optics. In order to achieve a contrast in surface sensitivity photon energies of 170 and 350 eV were applied to investigate the Si 2*p* core level and 350 and 510 eV for the C 1*s* core level, respectively. This results in C 1*s* and Si 2*p* core level spectra with comparable surface sensitivity. The effective sampling depths λ_{eff} are 3.0 and 4.6Å for the spectra taken at lower and higher photon energy, respectively.[43]

The effect of annealing of the surfaces at temperatures as high as 990 °C in UHV was also studied using SXPS and LEED. Heating of the samples was accomplished by electron bombardment of the backside of the sample holder. The sample temperature was monitored by means of a pyrometer with the emissivity adjusted to that of the sample holder made of molybdenum ($\epsilon=0.25$). Calibration measurements

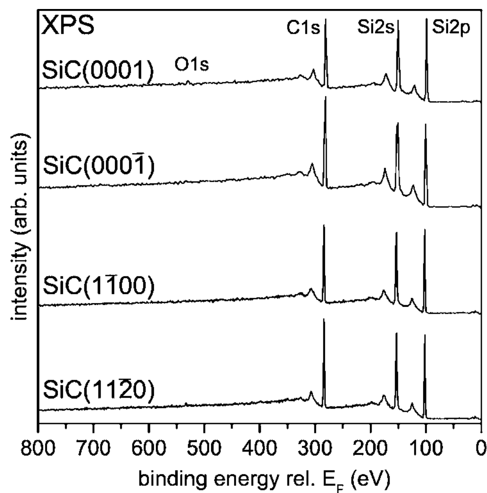

FIG. 1. XPS survey scans of H-terminated 6*H*-SiC(0001), 6*H*-SiC(000$\bar{1}$), 4*H*-SiC(1$\bar{1}$00), and 4*H*-SiC(11$\bar{2}$0).

using a Ni/Cr-Ni thermocouple have shown that the temperature accuracy is about 30 °C. At each temperature the surfaces were annealed for two minutes. During annealing the chamber pressure increased but did not exceed 2×10^{-8} mbar.

III. RESULTS AND DISCUSSION

A. Characterization by XPS and LEED

In Fig. 1 XPS survey scans of four hydrogen terminated SiC surfaces of different orientation are compared: 6*H*-SiC(0001), 4*H*-SiC(11$\bar{2}$0), 4*H*-SiC(1$\bar{1}$00), and 6*H*-SiC(000$\bar{1}$). The spectra are normalized in such a way that the Si 2*p* core levels have the same intensity. In all cases, commonly observed contaminants like oxygen, fluorine, and hydrocarbons are removed by the hydrogenation process so that their signals are at or below the detection limit of approximately 0.2 atomic percent. On the (0001) plane the Si 2*p* core line is more intense than the C 1*s* line, but the reverse situation is observed on the (000$\bar{1}$) surface, although both surfaces are stoichiometric. The observed Si 2*p*/C 1*s* ratios are due to the layered structure of SiC.[45] On SiC(0001) all the C atoms of a given bilayer are located below the Si atoms of the same bilayer and, therefore, the photoelectrons of the C 1*s* core level experience an additional damping. Since the arrangement of atoms is reversed on the carbon face, we observe the reversed Si 2*p*/C 1*s* ratio. On the other hand, the intensity ratios measured on the nonpolar surfaces (see Fig. 1) show intermediate values indicating that they are stoichiometric.

Figure 2 displays LEED patterns of the hydrogen-saturated 4*H*-SiC(1$\bar{1}$00) surfaces. The (1×1) unit mesh of the reciprocal lattice is indicated by a rectangle. The short side of the rectangle runs parallel to the *c* axis direction and the long side is oriented parallel to the [11$\bar{2}$0] direction. In addition, Fig. 2 shows a top view of the ideal, unreconstructed 4*H*-SiC(1$\bar{1}$00) surface indicating the size and orientation of the (1×1) unit cell. It is evident from Fig. 2 that the H-terminated 4*H*-SiC(1$\bar{1}$00) surfaces possesses an unreconstructed (1×1) periodicity. The diffraction spots exhibit some streakiness in the direction parallel to the *c* axis, which probably points towards a tendency for faceting in this direction. In accordance with the crystal structure of 4*H*-SiC, the LEED pattern lacks rotational symmetry, but shows a mirror symmetry with a mirror plane parallel to the *c* axis direction [0001].

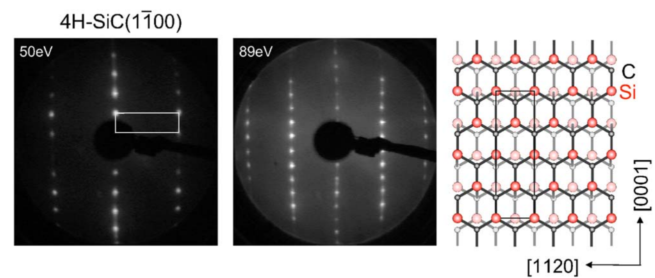

FIG. 2. (Color online) LEED patterns of H-terminated 4*H*-SiC(1$\bar{1}$00) taken at different electron energies. The rectangle inside the diffraction image indicates the (1×1) unit mesh of the reciprocal lattice. Also shown is a top view of the unreconstructed 4*H*-SiC(1$\bar{1}$00) surface indicating the (1×1) unit cell. Dark filled circles and dark lines indicate atoms and bonds of the top surface layer, respectively, while lighter shading is used for the second layer.

LEED patterns of the hydrogen-saturated 4*H*-SiC(11$\bar{2}$0) surfaces are shown in Fig. 3. Again, the (1×1) unit mesh of the reciprocal lattice is indicated by a rectangle with the short side of the rectangle running in *c* axis direction. The long side of the unit mesh in reciprocal space is now oriented parallel to the [1$\bar{1}$00] direction. Figure 2 also shows a top view of the ideal, unreconstructed 4*H*-SiC(11$\bar{2}$0) surface indicating the size and orientation of the (1×1) unit mesh. Again, it is evident from the diffraction image that the H-terminated surfaces is unreconstructed exhibiting (1×1) periodicity. Unlike the (1$\bar{1}$00) surface the diffraction spots are sharp without any noticeable streakiness.

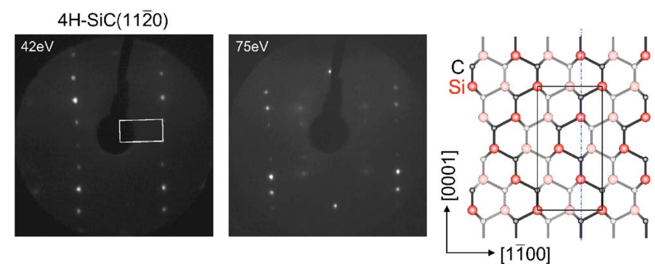

FIG. 3. (Color online) LEED patterns of H- terminated 4*H*-SiC(11$\bar{2}$0) taken at different electron energies. The rectangle inside the diffraction image indicates the (1×1) unit mesh of the reciprocal lattice. Also shown is a top view of the unreconstructed 4*H*-SiC(11$\bar{2}$0) surface indicating the (1×1) unit cell. Dark filled circles and dark lines indicate atoms and bonds of the top surface layer, respectively, while lighter shading is used for the second layer. The vertical line indicates the position of a glide-plane.

As expected from the symmetry of the crystal lattice, the LEED pattern of 4*H*-SiC($11\bar{2}0$) lacks rotational symmetry. In addition, the surface is also missing mirror symmetry. The only remaining symmetry of the surface is a glide-plane symmetry with the glide-plane indicated by the dash-dotted line in Fig. 3.

The presence of glide-plane symmetries is well known to lead to systematic extinctions of diffraction spots. This is also observed in the present case. In particular, spots (kl) with $k=0,\pm 3$ and $l=\pm 1,\pm 2,\pm 3$ were observed to be absent. A diffraction pattern shown by King *et al.*[48] obtained from 6*H*-SiC($11\bar{2}0$)$-(1\times 1)$ also shows indications for similar systematic spot extinctions. These are due to the fact that for structures with glide-plane symmetries the structure factor $S(k,l)$ becomes zero for certain combinations of k and l due to destructive interference of partial waves scattered by the individual atoms in the unit mesh. The structure factor $S(k,l)$ of a given diffraction spot indexed (kl) is given by[49]

$$S(k,l) = \sum_p f_p \exp(i\mathbf{s}_{kl}\cdot \mathbf{R}_p) \tag{1}$$

where the parallel momentum transfer $\mathbf{s}_{kl}=k\mathbf{g}_1+l\mathbf{g}_2$ is the two-dimensional reciprocal lattice vector of the surface lattice corresponding to the diffraction spot indexed (kl). $\mathbf{R}_p$ and f_p are the position and the atomic form factor of the pth atom in the unit cell, respectively. The sum runs over all atoms in the unit cell. Calculating the structure factor given in Eq. (1) shows that for the unreconstructed 4*H*-SiC($11\bar{2}0$) surface spots with indices (kl) satisfying the conditions $k=3n$, n integer and $l=4n+i$, n integer and $i=1,2,3$ are absent. This agrees well with the experimental observations. Note that these systematic spot extinctions are strictly fulfilled for normal incidence of the electron beam. Slight misalignment of the sample can lead to an increase in intensity of otherwise invisible beams. No particular effort was made in the present work to exactly align the sample for normal incidence.

In conclusion, annealing 4*H*-SiC($11\bar{2}0$) and ($1\bar{1}00$) surfaces in ultra-pure hydrogen results in clean, stoichiometric and unreconstructed surfaces, which is in accordance with the observations made with the hexagonal {0001} surfaces of 6*H*-SiC.[37–45]

B. Highly resolved core level spectra

The discussion of highly resolved core level spectra obtained with synchrotron radiation from the hydrogen terminated surfaces in this section aims at an identification of chemically shifted surface components. The final goal is to develop structural models for the H-terminated 4*H*-SiC($11\bar{2}0$) and ($1\bar{1}00$) surfaces. As will be seen in the following discussion, the identification of surface components in the Si 2*p* spectra is much more complicated than for the C 1*s* spectra. Therefore, we shall first concentrate on the latter.

Figure 4 compares C 1*s* core level spectra of four different H-terminated SiC surfaces: 6*H*-SiC($000\bar{1}$) (C-face), 4*H*-SiC($11\bar{2}0$), 4*H*-SiC($1\bar{1}00$), and 6*H*-SiC(0001) (Si-face).

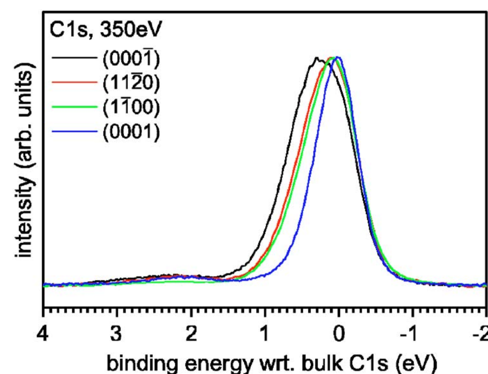

FIG. 4. (Color online) Comparison of C 1*s* core level spectra of H-terminated SiC surfaces taken at 350 eV. The binding energy is given with respect to the bulk component.

The spectra of the basal planes have been discussed elsewhere.[43] The binding energy scale is given with respect to the bulk contribution which was determined using a peak fit routine as described below and in Ref. 43. It is evident from Fig. 4 that the main peak is broadest for the C-face and and most narrow for the Si-face. This is due to the fact that in the first case the main peak is made up of two components due to bulk emission and C-H entities, respectively.[43] No C-H bonds are expected on the Si-face which consequently shows a narrow line in the C 1*s* spectrum. For 4*H*-SiC($11\bar{2}0$) and SiC($1\bar{1}00$) we observe strongly asymmetric C 1*s* peaks (see Fig. 4) with a total width somewhere between the polar surfaces indicating that C-H bonds are present but to lesser extend than on the C-face. Considering that the nonpolar surfaces are made up of both Si and C atoms this is quite understandable.

Figure 5 shows highly resolved C 1*s* core level spectra of 4*H*-SiC($11\bar{2}0$) and 4*H*-SiC($1\bar{1}00$) after hydrogenation taken with two different photon energies as described in Sec. II. The experimental data are shown as open circles. The main lines show a clear asymmetry towards higher binding energy. In addition there is a weak peak located around 2.2 eV higher binding energy. Both, the asymmetry and the weak extra peak are reduced in intensity when increasing the photon energy from 350 eV (upper spectrum) to 510 eV (lower spectrum), i.e., when decreasing the surface sensitivity of the measurement.

The result of a deconvolution of the spectra into different components is shown in Fig. 5 as well. The individual peaks were modeled using Voigt lines, i.e., a convolution of a Lorentzain with a Gaussian distribution. For all components the Lorentzian width ω_L was 0.18 ± 0.01 eV. Prior to curve fitting a linear background was subtracted from the data. In some cases a Shirley background[50] was also tested, leading to practically identical results.

The C 1*s* spectra are made up of three components. Their fit parameters are collected in Table I. The behavior of these components upon changing the photon energy reveals that two of them are due to emission from the surface and one is due to emission from the bulk SiC. The latter component is labeled "SiC." The surface component labeled "Si_3C-H" has a chemical shift of 0.42 ± 0.03 eV in good agreement with the

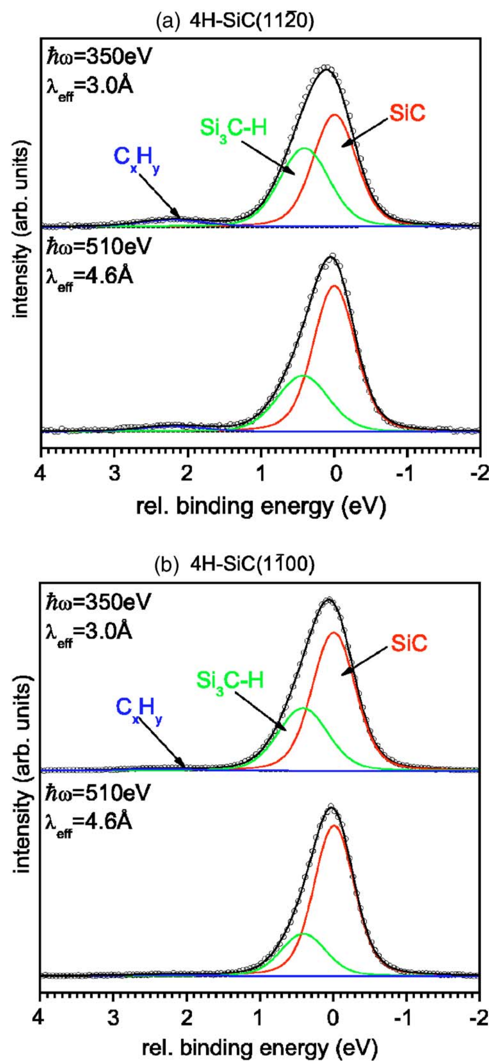

FIG. 5. (Color online) C 1*s* core level spectra of (a) 4*H*-SiC($11\bar{2}0$) and (b) 4*H*-SiC($1\bar{1}00$) taken at two different photon energies. The graphs also show the results of a deconvolution of the spectra into different components. The binding energy is given with respect to the bulk component.

value of 0.47±0.03 eV observed on the C-face.[43] Therefore, this component is assigned to carbon atoms bound to three silicon atoms and one hydrogen atom. Di- and trihydrides which would then be expected to lead to signals with chemical shifts of approximately 0.84 and 1.26 eV are obviously below the detection limit. Note that the Gaussian width of the monohydride component (Si_3C-H) is larger by 0.15 eV (see Table I) than that of the bulk component (SiC). This somewhat increased Gaussian width (by approximately 20%) must be due to a stronger inhomogeneous and/or phonon broadening at the surface. Similar ω_G values were observed for H-terminated {0001} surfaces of 6*H*-SiC.[40,43] Note that the relative intensity of the monohydride component with respect to the bulk component (0.52 at λ_{eff}=3.0 Å and 0.31 at λ_{eff}=4.6 Å) for 4*H*-SiC($1\bar{1}00$) is somewhat smaller than what is observed on 4*H*-SiC($11\bar{2}0$) (0.76 at λ_{eff}=3.0 Å and 0.46 at λ_{eff}=4.6 Å). However, as will be discussed in detail below, they agree well with estimates based on a simple layer attenuation models for certain surface structures.

The second chemically shifted component labeled "C_xH_y" at 2.20–2.35 eV with respect to the bulk component (cf. Table I) is due to a minute (few percent of a monolayer) hydrocarbon contamination which results from the storage of the sample in the vacuum transport vessel for up to two days.[40,43] The Gaussian width of this component, which on account of its small intensity is difficult to determine exactly, is approximately 1 eV which agrees well with values observed for hydrocarbon contaminations on SiC surfaces[40,43] and seems to indicate that these carbon atoms are in a more disordered arrangement than those giving rise to the other components in the C 1*s* spectrum.

Si 2*p* core level spectra of the four different H-terminated SiC surfaces are compared in Fig. 6. All spectra were taken with the same photon energy as the C 1*s* core level spectra shown in Fig. 4. The monochromator setting was not changed between the measurements of the C 1*s* and Si 2*p* core level spectra. Therefore, it is valid to give the binding energy in Fig. 6 with respect to the C 1*s* bulk line thus providing a reliable common energy reference.

The Si 2*p* core level spectrum of 6*H*-SiC($000\bar{1}$) is a single spin-orbit split doublet[43] which accounts for emission from the bulk. On the other hand, the Si 2*p* core level spectrum obtained from the H-terminated 6*H*-SiC(0001) surface shows an asymmetric broadening towards higher binding energy which has already been discussed in a previous publication.[43] The asymmetric shape is independent of doping type and doping concentration. Consequently an asymmetric broadening due to inhomogeneous band bending can be excluded. The asymmetry can also not be caused by the presence of Si-O bonds because the samples were free of oxygen as was demonstrated in Fig. 1. Therefore, it must be concluded that this asymmetric broadening is due to the Si atoms at the surface. As observed with the C 1*s* spectra shown in Fig. 4, the Si 2*p* spectra of the nonpolar surfaces show an asymmetric shape that lies between what is observed for the C-face and the Si-face. This further supports the explanation of the asymmetric line shape by Si atoms at the surface.

Figure 7(a) depicts Si 2*p* spectra of H-terminated 4*H*-SiC($11\bar{2}0$) measured with two different photon energies. Comparing the two spectra it is evident that reducing the surface sensitivity reveals a slight reduction of the high binding energy shoulder of the Si 2*p* core level. This corroborates the conclusion that the Si 2*p* core level spectrum contains a surface component at higher binding energy although the chemical shift must be rather small. Indeed, fitting the spectra with only one spin-orbit split doublet leads to unsatisfactory results. The results of a deconvolution of the spectra into two components with the high binding energy component being the surface component are also shown in Fig. 7(a). As a constraint the surface to bulk intensity ratio was set to the values obtained from the C 1*s* core level spectra. This assumption is justified by the fact that the surfaces were observed to be stoichiometric with a Si:C ratio of 1:1 and unreconstructed. Therefore, if the hydrogenation process leads to a saturation of dangling bonds on the surface equal num-

TABLE I. Summary of chemical shifts (ΔE_b) and Gaussian widths (ω_G) in eV of the different components observed in C 1*s* and Si 2*p* spectra. The Gaussian widths of the bulk components after annealing to 990 °C are given in parentheses. Lorentzian widths were 0.18±0.01 eV for the C 1*s* core level and 0.11±0.01 eV for the Si 2*p* core level, respectively.

		$4H$-SiC($11\bar{2}0$)		
Level	Label	ΔE_b	ω_G	Assignment
C 1*s*	SiC	0	0.59±0.03	SiC bulk
			(0.75±0.03)	
	Si_3C-H	0.42±0.03	0.72±0.05	C monohydride
	C_xH_y	2.2±0.1	1.0±0.1	hydrocarbons
	S_C1	−0.75±0.05	0.57±0.05	—
	S_C2	0.80±0.05	0.85±0.1	—
	S_C3	1.75±0.1	1.2±0.1	graphitic patches
Si 2*p*	SiC	0	0.52±0.03	SiC bulk
			(0.64±0.03)	
	C_3Si-H	0.23±0.03	0.67±0.05	Si monohydride
	$S_{Si}1$	−0.28±0.05	0.73±0.06	—
	Si-O	0.6±0.05	0.80±0.05	C_3Si-O suboxide

		$4H$-SiC($1\bar{1}00$)		
Level	Label	ΔE_b	ω_G	Assignment
C 1*s*	SiC	0	0.56±0.03	SiC bulk
			(0.80±0.03)	
	SiC-H	0.42±0.03	0.67±0.05	C monohydride
	C_xH_y	2.35±0.1	1.0±0.1	hydrocarbons
	S_C1	−0.70±0.05	0.57±0.05	—
	S_C2	0.85±0.05	0.85±0.1	—
	S_C3	1.75±0.1	1.2±0.1	graphitic patches
Si 2*p*	SiC	0	0.57±0.03	SiC bulk
			(0.67±0.03)	
	C_3Si-H	0.23±0.03	0.63±0.05	Si monohydride
	$S_{Si}1$	−0.28±0.05	0.73±0.06	—
	$S_{Si}2$	−1.38±0.10	0.75±0.07	excess Si
	Si-O	0.6±0.05	0.80±0.05	C_3Si-O suboxide

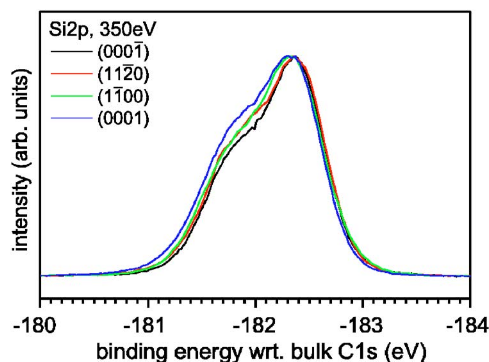

FIG. 6. (Color online) Comparison of Si 2*p* core level spectra of H-terminated SiC surfaces taken at 350 eV. The binding energy is given with respect to the bulk component of the corresponding C 1*s* core level spectra.

bers of C-H and Si-H entities will be formed. The chemical shifts and Gaussian widths are listed in Table I. The component due to photoelectrons emitted from the bulk is labeled "SiC." The surface component labeled "C_3Si-H" with a chemical shift of 0.23±0.03 eV is tentatively assigned to Si atoms bound to three carbon atoms and one hydrogen atom. Its chemical shift agrees well with the value of 0.2 eV determined for surface component assigned to the same configuration on $6H$-SiC(0001)-(1×1)-H.[40,43] In agreement with the fits of the C 1*s* spectra discussed above nothing points to the presence of di- and trihydrides. The Gaussian widths of the two components (see Table I) show the same behavior as observed with the C 1*s* core level spectra, i.e., the surface component has a Gaussian width around 0.15 eV larger than the bulk component indicating a stronger inhomogeneous and/or phonon broadening at the surface.

Si 2*p* spectra collected from the H-saturated $4H$-SiC($1\bar{1}00$) surface are plotted in Fig. 7(b). Again, the only

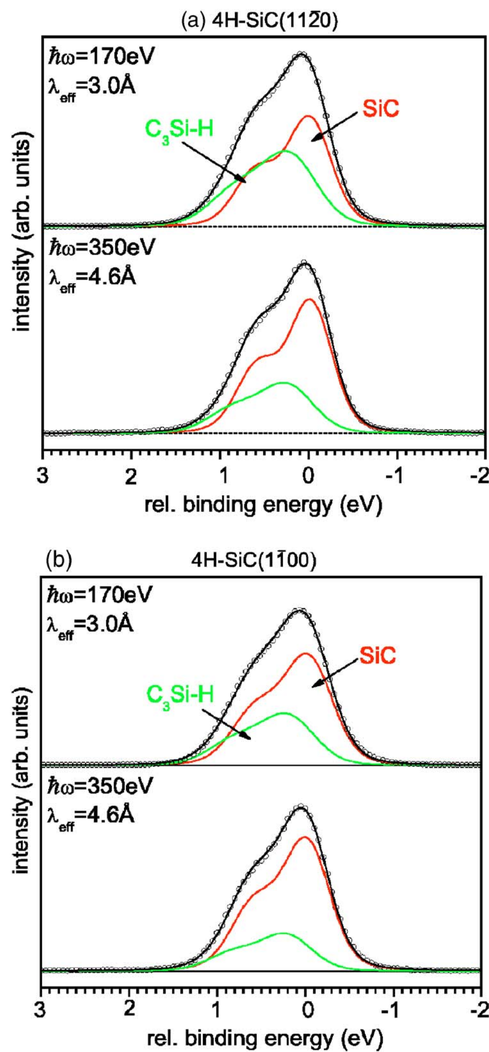

FIG. 7. (Color online) Si 2p core level spectra of (a) 4H-SiC(11$\bar{2}$0) and (b) 4H-SiC(1$\bar{1}$00) taken at two different photon energies. The graphs also show the results of a deconvolution of the spectra into two spin-orbit split doublets. The binding energy is given with respect to the bulk component.

noticeable difference between the two experimental spectra is a slight reduction of the shoulder at higher binding energy at higher photon energy. The spectra were also modeled with two spin-orbit split doublets which are labeled "SiC" and "C_3Si-H" and which we suggest to have the same origin as the two components obtained for 4H-SiC(11$\bar{2}$0). As a constraint the chemical shift of the monohydride component has been set to the value of 0.23 eV determined for 4H-SiC(11$\bar{2}$0). The chemical shifts and Gaussian widths of the two components determined for H-terminated 4H-SiC(1$\bar{1}$00) are also collected in Table I. In compliance with the C 1s spectra, the relative intensity of this component with respect to the bulk component was determined as 0.50 at λ_{eff}=3.0 Å and 0.30 at λ_{eff}=4.6 Å. The Gaussian widths (see Table I) show the same behavior as seen for the corresponding components in the Si 2p core level spectra of 4H-SiC(11$\bar{2}$0) as well as in the C 1s spectra discussed above. Again, di- and trihydrides are not observed.

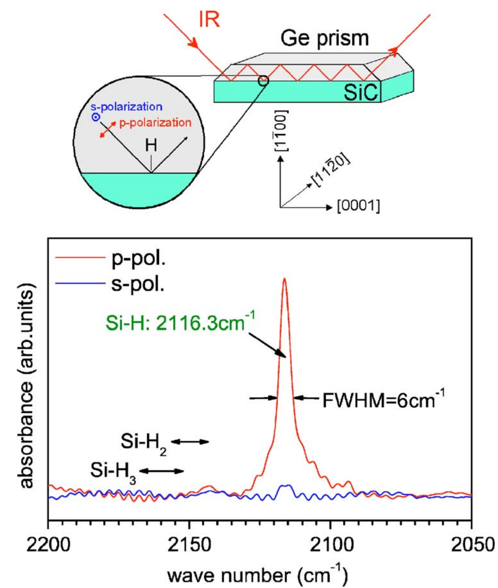

FIG. 8. (Color online) FTIR-ATR spectra of the Si-H stretch mode region taken from H-terminated 4H-SiC(1$\bar{1}$00). The sketch above the spectrum shows the measurement geometry used for this experiment.

In the light of the rather small intensity of the silicon monohydride component in the Si 2p spectra of H-terminated 4H-SiC(1$\bar{1}$00) we have also investigated this surface for Si-H bonds by Fourier-transform infrared absorption spectroscopy in the attenuated total reflection mode (FTIR-ATR). Figure 8 shows FTIR-ATR spectra of the Si-H stretch mode region. Also shown is a sketch of the measurement geometry indicating the orientation of the electric field vector of the IR radiation with respect to the crystal lattice. The spectrum recorded in p polarization shows a sharp Si-H stretch mode at 2116.3 cm^{-1} which is proof of Si-H monohydrides on the surface. Dihydrides and trihydrides which are expected[33,34,51] to lead to signals at around 2150 and 2170 cm^{-1}, respectively, are absent. This supports the interpretation of the Si 2p spectra above. In addition, the Si-H stretch mode is visible only in p polarization and absent in s polarization. As can be seen from the drawing in Fig. 8, the sample was oriented in such a way that the electric field vector in s polarization was parallel to the [11$\bar{2}$0] direction. Thus, the Si-H bonds are oriented in a way that their dipole moment has a vanishing component in in that direction.

As can be seen from the discussion above, the analysis of the photoemission data of H-terminated polar 6H-SiC0001 surfaces[40,43] and nonpolar 4H-SiC(1$\bar{1}$00) and (11$\bar{2}$0) surfaces leads to consistent results. The saturation of surface dangling bonds on SiC surfaces with hydrogen leads to chemically shifted components in the C 1s and Si 2p spectra at average values of +0.45 eV and +0.22 eV, respectively. The components are assigned to "Si_3C-H" and "C_3Si-H" configurations, respectively. Of the elements under consideration, Si has the smallest electronegativity of 1.8, carbon the largest (2.5) and hydrogen a value in between (2.1).[52] Replacing a C-Si bond by a C-H bond should, there-

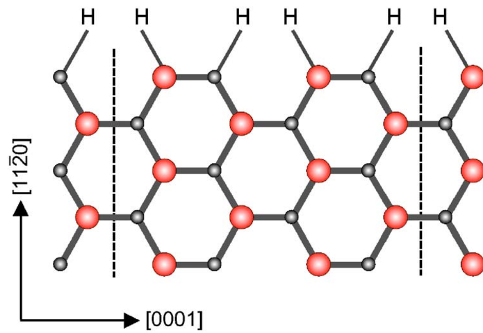

FIG. 9. (Color online) Side view projection of the H-terminated 4*H*-SiC(11$\bar{2}$0) surface. The vertical dashed lines indicate the dimension of the (1×1) unit cell in the direction of the *c* axis.

fore, lead to higher C 1*s* core level binding energy, which agrees with the experimental finding. On the other hand, a shift to lower binding energy is expected for the Si 2*p* core level. This is at variance with the core level data. As was shown in previous work on amorphous a-$Si_{1-x}C_x$:H,[53] the replacement of a Si-Si bond by a Si-C bond increases the Si 2*p* core level binding energy by 0.3 eV. At the same time, the replacement of a C-C bond by a C-Si bond causes the C 1*s* core level binding energy to shrink by 0.35 eV. Taking into account the electronegativities of the elements Si, C, and H we estimate expected chemical shifts of −0.17 eV for the "C_3Si-H" configuration and +0.15 eV for the "Si_3C-H" configuration, respectively. The latter value differs from the experimental value by 0.3 eV which may indicate that the observed shift is not purely due to initial state effects. Therefore, we suggest that final state effects may be responsible for the unexpected sign of the Si 2*p* surface chemical shift. It is conceivable that screening of the core hole by extra-atomic relaxation is less effective for surface atoms than for bulk atoms. Then a small chemical shift due to initial state effects may be overridden by final state effects and a reversed net chemical shift may be observed.

C. Structure models of H-terminated nonpolar surfaces

The spectroscopic data discussed above can be used to develop structure models for the hydrogenated *a* planes of 4*H*-SiC. In the case of 4*H*-SiC(11$\bar{2}$0) this is rather simple. XPS has shown that the surface is stoichiometric with a Si:C ratio of 1:1. The LEED data indicate that the surface has a (1×1) periodicity and using SXPS we have determined chemically shifted components which were assigned to silicon and carbon monohydrides (C_3Si-H and Si_3C-H). These experimental results are compatible with the structure depicted in Fig. 9. It consists of a simple bulk-terminated and unreconstructed surface on which one dangling bond per surface atom (eight per unit cell, see also Fig. 3) is saturated by hydrogen in the form of monohydrides. The surface should therefore be referred to as 4*H*-SiC(11$\bar{2}$0)-(1×1)-8H structure. Using a simple layer attenuation model for estimating the relative intensities of the surface components with respect to the bulk components values of 0.68 and 0.40 for effective sampling depths λ_{eff} of 3.0 and 4.6 Å are obtained for this model. These numbers agree fairly well with the experimental results of 0.76 and 0.46, respectively. The surface to bulk ratios quoted above are lower than the corresponding ratios observed on the polar {0001} surfaces.[43] This is due to the fact that on the polar surfaces only one type of monohydrides is present, i.e., the Si face contains Si-H only and the carbon face is terminated by C-H. On the other hand, the ideal hydrogenated 4*H*-SiC(11$\bar{2}$0) surface contains Si and C monohydrides in equal amounts, which reduces the surface to bulk ratio in the individual corelevel spectra.

In the case of H-terminated 4*H*-SiC(1$\bar{1}$00) the number of possible (1×1) surfaces is more abundant as shown in Fig. 10. In order to identify the correct structure, the number of dangling bonds has to be considered which are formed when the surface is created and which are saturated by hydrogen. As can be seen from Fig. 10, the configuration of Fig. 10(a) contains equal amounts of Si and C atoms with one H-saturated dangling bond. The surfaces shown in Figures 10(b) and 10(c) contain equal amounts of mono- and dihydrides. Finally, the surface shown in Fig. 10(d) is made up of dihydrides only. All these (1×1) surfaces fulfill the requirement of a Si:C ratio of 1:1. However, only the configuration shown in Fig. 10(a) is compatible with the fact that only monohydrides were observed in the SXPS and FTIR-ATR spectra. The structure should be referred to as 4*H*-SiC(1$\bar{1}$00)-(1×1)-4H structure.

Closer inspection of this structure reveals that it is made up of Si-face and C-face nano-facets. Applying a layer attenuation model to this structure yields theoretical estimates for the monohydride to bulk intensity ratio of 0.42 and 0.28 at λ_{eff} of 3.0 and 4.6 Å, respectively, which is in fair agree-

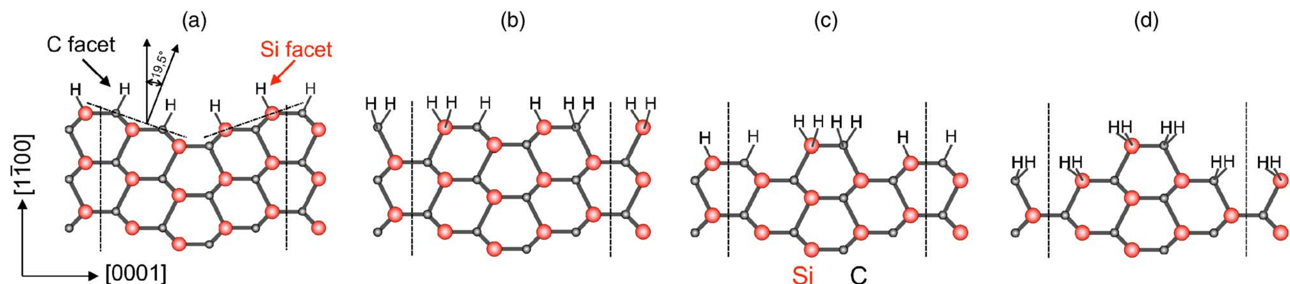

FIG. 10. (Color online) Side view projection of the four different possible structures of H-terminated 4*H*-SiC(1$\bar{1}$00) with (1×1) periodicity. The vertical dashed lines indicate the dimension of the (1×1) unit cell in *c* axis direction.

ment with the experimental values (0.50 and 0.30). Note that these ratios are smaller than on the (11$\bar{2}$0) surface because only one half of the atoms of each element in the surface layer are bound to hydrogen and the other half is in a chemical environment equivalent to the bulk (see Fig. 10).

The Si-H and C-H bonds of the proposed 4*H*-SiC(1$\bar{1}$00)-(1×1)-4H structure [see Fig. 10(a)] are not perpendicular to the macroscopic surface plane. The angle between the Si-H and C-H bonds and the surface normal amounts to 19.5 deg. However, these bonds are lying in the drawing plane and, therefore, their dipole moment has a zero component in [11$\bar{2}$0] direction. In agreement with that, the Si-H stretch mode was only observed in *p* polarization but not in *s* polarization with the electric field vector parallel to that direction.

Rauls *et al.*[27–29] used a self-consistent charge density-functional based tight-binding method (SCC-DFTB) to study the energetics of the clean *a* planes of 2*H*-, 4*H*-, and 6*H*-SiC, i.e., surfaces without dangling bond saturation. They predict that a structure similar to the one shown in Fig. 10(a) is energetically favorable compared to the structures in Figs. 10(b) and 10(c). Considering the number of dangling bonds of the individual structures this result is not surprising. However, in the presence of hydrogen this could be different. The Si-H and C-H bonds of the dihydrides in Figs. 10(b)–10(d) are not parallel to the paper plane but tilted. The formation of Si-Si and C-C bonds in the surface seems possible which would lead to a (2×1) reconstruction. However, this was not observed even after thermal desorption of hydrogen from the surface (see below).

D. Thermally induced surface reactions

It was recently reported by Virojanadara *et al.*[20] that annealing *ex situ* cleaned 4*H*-SiC(1$\bar{1}$00) and 4*H*-SiC(11$\bar{2}$0) surfaces at 1000 °C leads to clean (oxygen free) and unreconstructed surfaces. The C 1*s* spectra obtained in this way contained quite intense chemically shifted surface components but their Si 2*p* spectra showed only a very weak surface component at −0.6 eV. This was taken as evidence for carbon enrichment on their surfaces which was supported by an increase of the carbon to silicon intensity ratio. This is in contradiction to the theoretical work by Rauls *et al.*[29] who proposed Si-rich reconstructions which are stable even under carbon rich conditions. Because the H-terminated SiC surfaces provide an oxygen-free and stoichiometric starting point we investigated in how far temperature induced surface reactions and reconstructions occur. This was accomplished by observing core level spectra and LEED patterns after annealing the surfaces at different temperatures up to 990 °C. However, for both 4*H*-SiC(1$\bar{1}$00) and 4*H*-SiC(11$\bar{2}$0) the surface periodicity was observed to remain unchanged (1×1) after all annealing steps.

Si 2*p* core level spectra of 4*H*-SiC(11$\bar{2}$0)-(1×1)-8H after annealing at various temperatures are depicted in Fig. 11(a). The Si 2*p* spectrum remains basically unchanged after annealing at 520 °C but indicates a slight broadening after annealing at 680 °C. Increasing the temperature to 820 °C leads to a slight asymmetry at the higher binding energy side. The Si atoms responsible for this asymmetric broadening are located at the surface because the strength of the asymmetry

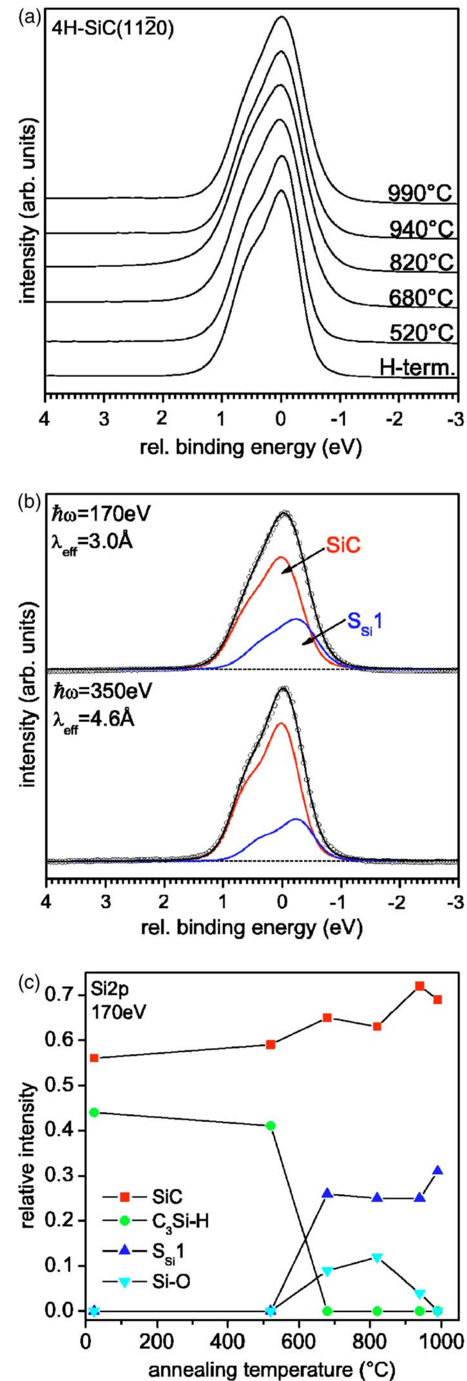

FIG. 11. (Color online) (a) Si 2*p* spectra taken at $\hbar\omega$=170 eV of 4*H*-SiC(11$\bar{2}$0)-(1×1)-8H after successive annealing steps in UHV. (b) Si 2*p* spectra taken at two different photon energies after annealing at 990 °C together with the result of a peak fit. (c) Relative intensities of the different components in the Si 2*p* core level spectra of 4*H*-SiC(11$\bar{2}$0)-(1×1)-8H taken at $\hbar\omega$=170 eV as a function of annealing temperature. The relative error in the intensities is estimated to be ±10%.

is lowered when the surface sensitivity is decreased by increasing the photon energy (not shown). Such an asymmetry at higher binding energy side is caused by the presence of small amounts of oxygen on the surface. It is known from our previous studies of 6*H*-SiC(0001) that the desorption of hydrogen occurs at temperatures of around 750 °C.[43] The desorption of hydrogen is likely to lead to silicon dangling bonds, which are very susceptible to oxidation by oxygen containing species in the residual gas of the ultrahigh vacuum (UHV) chamber. The presence of small amounts of oxygen ($\leqslant 0.15$ monolayers) was also established by XPS survey scans. The O-induced asymmetry is reduced by annealing at higher temperatures indicating a desorption of the intermediate oxygen contaminants. In addition to this observation, the low-energy flank of the Si 2*p* main line appears less steep than observed on the hydrogenated sample indicating the presence of a component at lower binding energy than bulk SiC. Varying the effective sampling depth reveals that the Si atoms responsible for this feature are located at the surface.

In order to gain more insight into the behavior of the core level spectra each of them was deconvoluted into a number of chemically shifted components. The chemical shifts and Gaussian widths of the components used are summarized in Table I. Figure 11(b) shows an example of such a peak fit to the Si 2*p* spectra taken after annealing at 990 °C. A chemically shifted surface component ($S_{\mathrm{Si}}1$) at -0.28 ± 0.05 eV is required to fit the spectra. Its Gaussian width amounts to 0.73 ± 0.06 eV. The Gaussian width of the bulk component increases due to the annealing so that it reaches a value of 0.64 ± 0.03 eV after the final annealing step (see Table I). A comparable behavior was observed with the polar basal planes.[43] Corresponding peak fits of the spectra acquired after annealing at lower temperatures included a surface component (Si-O) located at 0.6 ± 0.05 eV relative binding energy with a Gaussian width of 0.80 ± 0.05 eV due to the intermediate oxygen contamination mentioned above. The evolution of the relative intensities of the components SiC, C_3Si-H, Si-O, and $S_{\mathrm{Si}}1$ in the Si 2*p* spectra taken with 170 eV photons with annealing temperature is displayed in Fig. 11(c). The relative intensity I_x^{rel} of a given component is defined as $I_x^{\mathrm{rel}} = I_x / \Sigma_y I_y$ where I_x is the intensity of component x and the sum runs over all components y including component x. It is evident that the components $S_{\mathrm{Si}}1$ and Si-O are formed at the same time as the mono-hydride component C_3Si-H vanishes. Note that the latter has disappeared completely at 680 °C. Si-O vanishes at the highest annealing temperature, whereas the surface component $S_{\mathrm{Si}}1$ remains present.

Figure 12(a) shows the corresponding C 1*s* spectra. No significant changes are observed after annealing at 520 °C except for a reduction of the minor hydrocarbon contamination. At 680 °C a shoulder appears at −0.7 eV. This shoulder remains basically unchanged by the subsequent annealing steps. On the other hand, heating the sample at 820 °C leads to an asymmetric broadening at higher binding energy, which is caused by a further chemically shifted component as discussed below. Finally, an additional signal shows up at around 1.75 eV with respect to the bulk component which is weak first but clearly discernible after annealing at 990 °C.

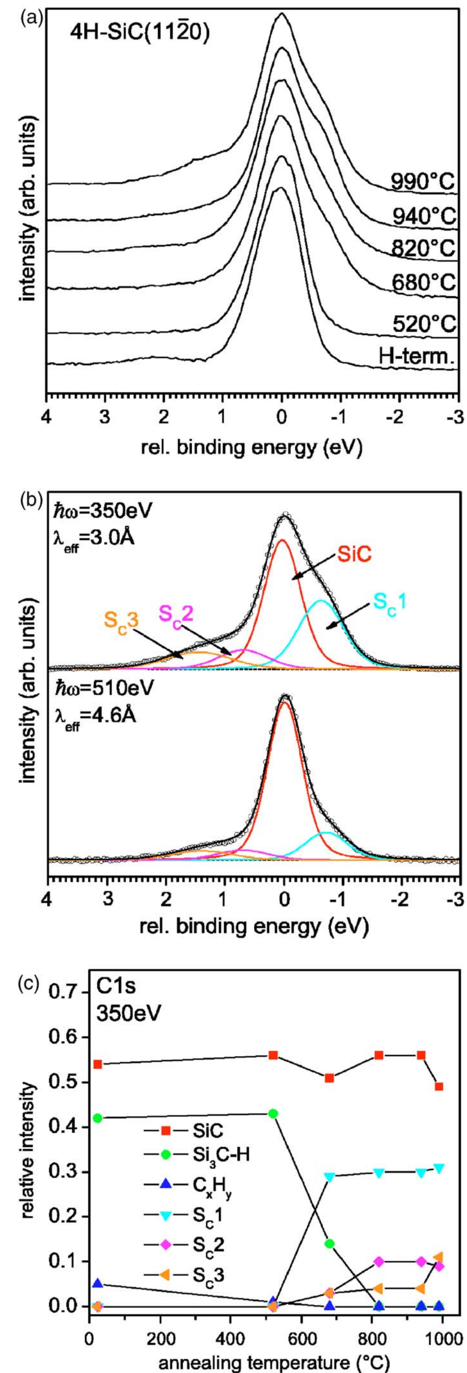

FIG. 12. (Color online) (a) C 1*s* spectra taken at $\hbar\omega = 350$ eV of 4*H*-SiC(11$\bar{2}$0)-(1×1)-8H after successive annealing steps in UHV. (b) C 1*s* spectra taken at two different photon energies after annealing at 990 °C together with the result of a peak fit. (c) Relative intensities of the different components in the C 1*s* core level spectra of 4*H*-SiC(11$\bar{2}$0)-(1×1)-8H taken at $\hbar\omega = 350$ eV as a function of annealing temperature. The relative error in the intensities is estimated to be ±10%.

Varying the photon energy reveals that all three additional components are due to carbon atoms located at the surface.

Figure 12(b) depicts a fit of the C 1*s* spectra taken after annealing at 990 °C. Four components were used: The bulk component (SiC) and three chemically shifted surface com-

ponents denoted S_C1, S_C2, and S_C3 with chemical shifts of -0.75 ± 0.05, 0.80 ± 0.05, and 1.75 ± 0.1 eV, respectively. The Gaussian widths are compiled in Table I. As observed with the Si 2*p* core level, the Gaussian width of the bulk component is increased after the annealing.

The evolution of the different chemically shifted components in the C 1*s* core level spectra taken at a photon energy of 350 eV can be seen in Fig. 12(c) where their relative intensities are plotted as a function of annealing temperature. It is evident from Fig. 12(c) that S_C1 is the first component which is formed and that its appearance is accompanied by a reduction of the carbon monohydride component (Si_3C-H). After the formation of S_C1 is completed, S_C2 starts to develop and the monohydride component vanishes completely at 820 °C. Note that the carbon mono-hydride component (Si_3C-H) survived longer than the silicon mono-hydride component (C_3Si-H), which had already disappeared after annealing at 580 °C [see Fig. 11(c)]. This is consistent with a stronger C-H bond as compared to the Si-H bond. At 820 °C, where S_C1 and S_C2 are fully developed and S_C3 is still small (4% of the whole C 1*s* signal) the intensity ratio $(S_C1+S_C2)/\mathrm{SiC}$ is 0.71, which is in good agreement with the monohydride to bulk ratio of 0.76 determined for the H-terminated surface. This seems to indicate that approximately one monolayer of carbon atoms is involved in the formation of the two surface components S_C1 and S_C2. Finally, S_C3 evolves after the completion of S_C1 and S_C2.

The microscopic origin of the chemically shifted components in the C 1*s* spectra as well as in the Si 2*p* spectra is hard to tell. A discussion of this matter will follow after the analysis of corresponding data obtained from 4*H*-SiC($1\bar{1}00$).

Figure 13(a) depicts Si 2*p* core level spectra taken from 4*H*-SiC($1\bar{1}00$)-(1×1)-4H after successive annealing steps in UHV. The behavior of the spectra is very similar to what was observed with 4*H*-SiC($11\bar{2}0$). The Si 2*p* spectrum is basically unaltered after annealing at 520 °C. It shows a slight broadening after annealing at 680 °C and as with 4*H*-SiC($11\bar{2}0$) a slight asymmetry at the higher binding energy side indicates the presence of oxygen on the surface. The O-induced asymmetry is reduced by annealing at higher temperatures indicating a desorption of the intermediate oxygen contaminants. The low-energy flank of the Si 2*p* main line appears less steep as compared to hydrogenated sample, again indicating the presence of a component at lower binding energy than bulk SiC. In addition, an extremely weak surface component at −1.3 eV is observed after annealing at 940 °C which was not present on the other surface.

As with 4*H*-SiC($11\bar{2}0$) the spectra were further analyzed by peak fitting. For the Si 2*p* spectra taken after annealing at 990 °C the result is plotted in Fig. 13(b). The spectrum consists of four components (see also Table I). One component (SiC) is assigned to emission from the bulk. The other components are due to emission from surface atoms and are located at -0.28 ± 0.05 eV ($S_{Si}1$), -1.38 ± 0.10 eV ($S_{Si}2$), and 0.60 ± 0.05 eV (Si-O). Their temperature dependence is plotted in Fig. 13(c). The behavior of the four components SiC, C_3Si-H, $S_{Si}1$, and Si-O is in agreement with the observations made on the ($11\bar{2}0$)-surface. The extremely weak component $S_{Si}2$ is only visible after annealing at 940 °C and amounts to ~1% of the integrated Si 2*p* intensity.

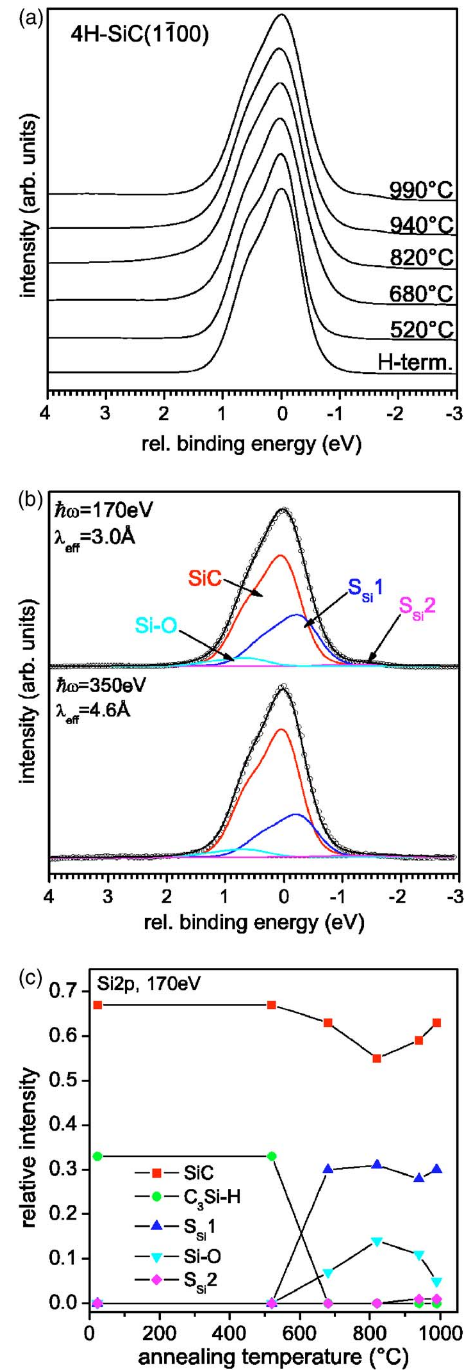

FIG. 13. (Color online) (a) Si 2*p* spectra taken at $\hbar\omega=170$ eV of 4*H*-SiC($1\bar{1}00$)-(1×1)-(1×1)-4H after successive annealing steps in UHV. (b) Si 2*p* spectra taken at two different photon energies after annealing at 990 °C together with the result of a peak fit. (c) Relative intensities of the different components in the Si 2*p* core level spectra of 4*H*-SiC($1\bar{1}00$)-(1×1)-(1×1)-4H taken at $\hbar\omega=170$ eV as a function of annealing temperature. The relative error in the intensities is estimated to be ±10%.

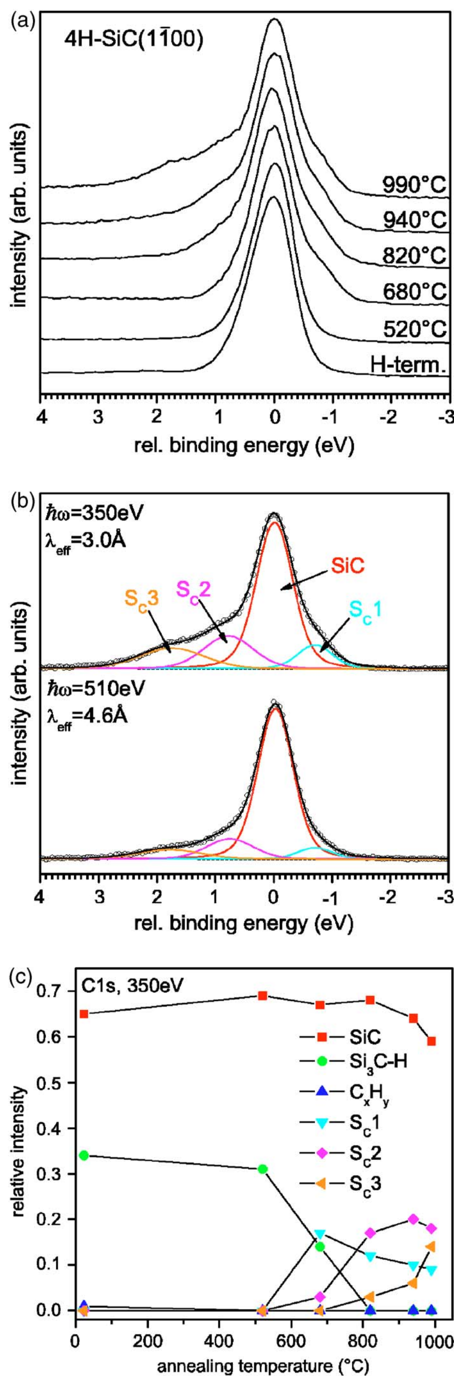

FIG. 14. (Color online) (a) C 1*s* spectra taken at $\hbar\omega$=350 eV of 4*H*-SiC(1$\bar{1}$00)-(1×1)-4H after successive annealing steps in UHV. (b) C 1*s* spectra taken at two different photon energies after annealing at 990 °C together with the result of a peak fit. (c) Relative intensities of the different components in the C 1*s* core level spectra of 4*H*-SiC(1$\bar{1}$00)-(1×1)-4H taken at $\hbar\omega$=350 eV as a function of annealing temperature. The relative error in the intensities is estimated to be ±10%.

The C 1*s* spectra are shown in Fig. 14(a). No major changes are observed after annealing at 520 °C. At 680 °C a shoulder becomes visible at −0.70 eV, which remains basically unchanged by annealing at higher temperatures. At 820 °C a shoulder appears at around 0.85 eV higher binding energy. Finally a further signal at around 1.75 eV with respect to the bulk component shows up after annealing at 990 °C. Variation of the photon energy reveals that all these additional components are due to atoms located at the surface.

Fitting results obtained for the C 1*s* spectra acquired after the final anneal at 990 °C are given in Fig. 14(b). The spectra were deconvoluted into four components as was done with the corresponding spectra of 4*H*-SiC(11$\bar{2}$0). The chemical shifts and Gaussian widths of the components are summarized in Table I. One component (SiC) is assigned to emission from the bulk. The others are surface components and are located at −0.70±0.05 eV (S_C1), 0.85±0.05 eV (S_C2) and 1.75±0.05 eV (S_C3). The evolution of the chemically shifted components with increasing temperature is displayed in Fig. 14(c). In agreement with the Si 2*p* spectra the temperature dependence of the different components is very similar to what was observed on the other a-plane. Again we note that the carbon mono-hydride component Si_3C-H survives longer than the silicon mono-hydride component in the Si 2*p* spectra.

As mentioned before, Virojanadara *et al.*[20] observed chemically shifted components in the C 1*s* core level spectra obtained after annealing *ex situ* cleaned, nonpolar 4*H*-SiC(1$\bar{1}$00) and 4*H*-SiC(11$\bar{2}$0). A temperature of 1000 °C was required to completely remove oxygen from the surfaces.[20] Two chemically shifted components are reported to exist in the C 1*s* spectra, which are located at −0.69±0.03 and 0.77±0.04 eV on 4*H*-SiC(1$\bar{1}$00) and −0.68±0.04 and 0.67±0.8 eV on 4*H*-SiC(11$\bar{2}$0), respectively. These values agree well with the shifts of the surface components S_C1 and S_C2 observed in the present study. The relative intensities of these surface components are quite similar. In addition, they also observe a further component with a chemical shift around 2 eV which is in fair agreement with our component S_C3. This component is weaker in the work of Virojanadara *et al.*[20] In fact, the intensity of their graphite component agrees more with what we observe at temperatures of 820 and 940 °C. A possible reason for this will be discussed below.

Despite the strong similarities between the C 1*s* spectra observed by Virojanadara *et al.*[20] and those obtained in the present work, the Si 2*p* spectra are markedly different in that the Si 2*p* spectra obtained by the Swedish group show only a weak surface component at −0.6 eV.[20] Its intensity is hard to estimate but it is of the order of 1/5 of our surface component $S_{Si}1$. The component was attributed to Si clusters or dispersed Si atoms in a carbon rich surface layer. In the present work the Si-2*p* core level spectra taken after annealing at 990 °C show a more intense surface related component ($S_{Si}1$) with a smaller chemical shift. In addition, XPS in our home laboratory as well as corresponding measurements using synchrotron radiation show no significant change in the C-Si ratio when the H-terminated samples are annealed up to 990 °C. Based on the structures presented above we estimate that half a monolayer of additional carbon atoms on H-SiC(11$\bar{2}$0) would increase the C 1*s*/Si 2*p* ratio in our experiment by approximately 15% which is not observed.

Therefore, we have to conclude that the stoichiometry of our surfaces is not strongly affected by the annealing procedure.

A possible explanation for the discrepancy between our results and the work of Virojanadara and Johansson[20] would be that the desorption of oxygen from the *ex situ* cleaned surfaces may commence via desorption of SiO. It is well known from Si surfaces that SiO_2 desorbs as SiO[54] via the reaction

$$Si + SiO_2 \rightarrow 2SiO\uparrow . \quad (2)$$

Therefore, if SiO desorption occurs via this reaction, cleaning the *ex situ* prepared surfaces by annealing in UHV could result in a silicon depleted surface, which in turn could be responsible for the absence of the surface component $S_{Si}1$ in the Si 2p spectra in Ref. 20.

A clear identification of the bonding arrangements responsible for the surface components observed after the individual annealing steps is difficult. Only the component Si-O, due to an intermediate oxygen contamination of the surface, can readily be identified. Its relative binding energy of 0.60 eV with respect to SiC bulk agrees well with previous observations made on wet-chemically cleaned SiC surfaces,[46,47] the silicate adlayer structure on 6*H*-SiC(0001),[55] or with oxidation studies of SiC surfaces.[22]

On account of its chemical shift of 1.75 eV and its large Gaussian width of 1.2 eV surface component S_C3 present in the C 1s spectra after annealing of the surfaces could be explained by the formation of graphitic patches on the surface. A similar component was observed in C 1s spectra after thermal desorption of hydrogen from H-terminated 6*H*-SiC(0001) at 820 °C[43] and after annealing of wet-chemically cleaned 6*H*-SiC(0001) surfaces at 950 °C.[56] In both studies a Si-rich $(\sqrt{3}\times\sqrt{3})R30°$ reconstruction with Si adatoms in T_4 sites[57] was observed after annealing. As discussed elsewhere[43,45] the graphitic patches observed simultaneously with the Si-rich $(\sqrt{3}\times\sqrt{3})R30°$ reconstruction are due to a disproportionation of the SiC surface which is necessary in order to provide the Si atoms forming the adatom structure at elevated temperatures. The graphitic component on the nonpolar surfaces is weaker in the work of Virojanadara *et al.*[20] This may be caused by differences in the temperature measurement but it may also indicate that graphitization is taking place only when most of the oxygen has been desorbed.

The tiny component $S_{Si}2$ at −1.38 eV observed on 4*H*-SiC(1$\bar{1}$00) after annealing at 940 °C and higher is likely to have an origin analogous to S_C3. Its chemical shift is indicative for elemental Si and the small intensity suggests that it is not located in any ordered part of the surface. Therefore, we suggest that it is due to a small amount of elemental Si in disordered areas of the surface in analogy to the S_C3 component.

The situation is more complicated for the remaining components S_C1, S_C2, and $S_{Si}1$. Chemically shifted surface components with shifts similar to our results were observed with reconstructed hexagonal SiC surfaces. In the case of the Si-rich $(\sqrt{3}\times\sqrt{3})R30°$ reconstruction on SiC(0001) a surface component with a chemical shift of −0.33 eV is observed which is caused by the Si atoms in the topmost bilayer.[43,56] These Si atoms are bound to three carbon atoms of the same bilayer and to the Si adatoms which reside in the T_4 position.[57] At the same time a surface component is observed at −0.45 to −0.60 eV in the C 1s spectrum[43,56] which is attributed to the carbon atoms of the topmost bilayer. The chemical shifts of −0.28 eV determined for $S_{Si}1$ and 0.65 eV for S_C1 may suggest that a similar bonding arrangement as observed with the Si-rich $(\sqrt{3}\times\sqrt{3})R30°$ reconstruction is present on the nonpolar surfaces as well. However, a Si adatom structure would likely lead to a surface periodicty deviating from the observed (1×1) peridicity. In addition, the spectra are lacking the signature of Si adatoms. Therefore, the possibilty of an adatom structure seems rather unlikely. Component S_C2 with a chemical shift of 0.75 eV suggests the presence of carbon atoms for which part of the Si neighbors has been replaced by C atoms. Since the replacement of one Si-C bond by one C-C bond would add a binding energy of 0.35 eV[53] one would estimate that these carbon atoms have forfeited two silicon neighbors which were replaced by bonds to carbon atoms.

But shifted surface components can not only be caused by different chemical environments. Surface buckling induced by charge transfer from surface cations to surface anions and accompanying surface core level shifts are well known for nonpolar (110) surfaces of III-V and II-VI semiconductors.[58] Surface buckling was predicted for clean nonpolar SiC surfaces.[29] While the possibility for buckling is constrained to the topmost Si and C atoms on 4*H*-SiC(1$\bar{1}$00) there are no constraints on 4*H*-SiC(11$\bar{2}$0). The buckling is induced by charge transfer from the silicon dangling bond to the carbon dangling bond, which causes the carbon atom (surface anion) to move outward and the silicon atom (surface cation) to move inward.[29] Due to the change in atomic charge of the relaxed surface atoms this would be likely to cause one chemically shifted surface component in both Si 2p and C 1s spectra with higher and lower binding energy than the bulk component, respectively. The analogon of this expectation is fulfilled for many nonpolar (110) surfaces of III-V and II-VI semiconductors[58] but it is not in agreement with the experimental observations made in our case in that the C 1s core level has more than one surface component and that the Si 2p surface component is located at lower binding energy than the bulk. This may indicate that the reality is more complicated on the SiC surfaces. On the other hand it is unclear whether or not the surface components in Si 2p and C 1s spectra belong to the same surface structure. Photoelectron spectroscopy is not a local technique, i.e., it averages over a large portion of the surface which could consist of patches of locally different surface structures. This may be clarified by STM.

IV. CONCLUSION

In this paper we have presented spectroscopic results obtained for hydrogenated 4*H*-SiC(11$\bar{2}$0) and (1$\bar{1}$00) surfaces. The C 1s core level spectra show a chemically shifted component at 0.42 eV higher binding energy which is assigned to carbon atoms in a Si_3C-H monohydride configuration. The

Si 2p core level spectra indicate the presence of chemically shifted component at 0.23 eV which is tentatively assigned to Si atoms in a C_3Si-H mono-hydride configuration. This assignment is in contradiction to expectations based on initial state effects but is supported by comparison with spectra obtained from the H-saturated basal planes. It is suggested that the final state effects are responsible for the surface shift to higher binding energy. Furthermore, the H-terminated surfaces are stoichiometric and unreconstructed. Structural models were proposed for the two hydrogen saturated nonpolar surfaces of 4H-SiC. The 4H-SiC$(11\bar{2}0)$-(1×1)-8H surface consists of a simple bulk truncation with one dangling bond per surface atom. The total of eight dangling bonds per unit cell are saturated by hydrogen. The 4H-SiC$(1\bar{1}00)$-(1×1)-4H surface consists of (0001) and $(000\bar{1})$ nano-facets. The dangling bonds on these nano-facets (a total of four per unit cell) are saturated in the form of Si-H and C-H monohydrides, respectively.

Thermal desorption of hydrogen from these surfaces leads to characteristic changes in the Si-2p and C 1s core level spectra, although the surface Si:C ratio and the (1×1) periodicity remain unaltered. A simple explanation for all the observed surface components cannot be provided. However, the results question the claims by Virojanadara and Johansson[20] that clean nonpolar surfaces of 4H-SiC are characterized by carbon enrichment. On the other hand, Si rich reconstructions predicted by the theoretical work of Rauls *et al.*[29] do not appear to be compatible with the experimental observations either. This is supported by our ongoing work on Si rich structures on 4H-SiC$(1\bar{1}00)$ which showed markedly different chemically shifted components in the Si 2p spectra than the spectra presented above.[31] It is suggested to address the open questions by investigations using scanning tunneling microscopy (STM) and LEED-$I(E)$ analyses.

One-dimensional metallic nano-wires have recently attracted much interest due to their expected unusual electronic properties[59] such as a deviation from the Fermi liquid behavior. One-dimensional nano-wires have previously been prepared on vicinal metal and semiconductor surfaces.[59] However, hybridization of the electronic states of the substrate with those of the nano-wire can adversly affect its electronic properties. For the large band gap semiconductor SiC we expect only a weak interaction between the substrate and the nano-wire. In addition, the nano-facet structures proposed for H-terminated H-SiC$(1\bar{1}00)$-(1×1)-4H are of particular interest because they provide a template for growing a high density of such wires. Furthermore, the distance between individual wires can be enlarged from 1 to 1.5 nm by going from 4H-SiC to 6H-SiC thus allowing to study the interaction between individual nano-wires as their distance is varied. The availability of such a modulated surface of a wide band gap semiconductor may open new possibilities to study the properties of metallic one-dimensional adsorbates.

ACKNOWLEDGMENTS

We thank the BMBF (contract 05 ES3XBA/5) for providing traveling funds for the measurements at BESSY II. M. Polcik is gratefully acknowledged for permitting the use of his spectrometer for the present studies. We also express our gratitude for support by the people at BESSY II, especially by W. Braun, H. Pfau, W. Mahler, and B. Zada. Finally, we would like to acknowledge fruitful discussions with U. Starke and L. Hammer.

*Corresponding author. Email: thomas.seyller@physik.uni-erlangen.de

†URL: http://www.tp2.uni-erlangen.de

[1] *Silicon Carbide—Recent Major Advances*, edited by W. Choyke, H. Matsunami, and G. Pensl (Springer, New York, 2004).

[2] D. L. Barrett, J. P. McHugh, H. M. Hobgood, R. H. Hopkins, P. G. McMullin, R. C. Clarke, and W. J. Choyke, J. Cryst. Growth **128**, 358 (1993).

[3] Y. M. Tairov, J. Cryst. Growth **29**, 83 (1995).

[4] R. A. Stein, P. Lanig, and S. Leibenzeder, Mater. Sci. Eng., B **11**, 69 (1992).

[5] Y. M. Tairov, Mater. Sci. Eng., B **29**, 83 (1995).

[6] N. Schulze, D. L. Barrett, G. Pensl, S. Rohmfeld, and M. Hundhausen, Mater. Sci. Eng., B **61–62**, 44 (1999).

[7] J. Takahashi and N. Ohtani, Phys. Status Solidi B **202**, 163 (1997).

[8] J. Takahashi, N. Ohtani, M. Katsuno, and S. Shinoyama, J. Cryst. Growth **181**, 229 (1997).

[9] T. Nishiguchi, T. Shimizu, M. Sasaki, S. Ohshima, and S. Nishino, Mater. Sci. Forum **353–356**, 69 (2000).

[10] D. Nakamura, I. Gunjishima, S. Yamaguchi, T. Ito, A. Okamoto, H. Kondo, S. Onda, and K. Takatori, Nature (London) **430**, 1009 (2004).

[11] T. Kimoto, T. Yamamoto, Z. Y. Chen, H. Yano, and H. Matsunami, Mater. Sci. Forum **338–342**, 543 (2000).

[12] T. Kimoto, H. Yano, S. Tamura, N. Miyamoto, K. Fujihira, Y. Negoro, and H. Matsunami, Mater. Sci. Forum **353–356**, 543 (2001).

[13] H. Yano, T. Kimoto, H. Matsunami, M. Bassler, and G. Pensl, Mater. Sci. Forum **338–342**, 1109 (2000).

[14] V. V. Afanas'ev, M. Bassler, and G. Pensl, Phys. Status Solidi A **162**, 321 (1997).

[15] G. Chung, J. Williams, K. McDonald, and L. Feldman, J. Phys.: Condens. Matter **16**, S1857 (2004).

[16] K. Gao, T. Seyller, L. Ley, F. Ciobanu, G. Pensl, A. Tadich, J. Riley, and R. Leckey, Appl. Phys. Lett. **83**, 1830 (2003).

[17] H. Yano, T. Hirao, T. Kimoto, H. Matsunami, K. Asano, and Y. Sugawara, IEEE Electron Device Lett. **20**, 611 (1999).

[18] H. Yano, T. Hirao, T. Kimoto, and H. Matsunami, Appl. Phys. Lett. **78**, 374 (2001).

[19] Y. Hoshino, S. Matsumoto, and Y. Kido, Surf. Sci. **531**, 295 (2003).

[20] C. Virojanadara and L. I. Johansson, Phys. Rev. B **68**, 125314 (2003).

[21] T. Seyller, K. Emtsev, R. Graupner, and L. Ley, Mater. Sci. Forum **457–460**, 1317 (2004).
[22] C. Virojanadara and L. Johanson, Surf. Sci. **505**, 358 (2002).
[23] C. Virojanadara and L. Johansson, Surf. Sci. **519**, 73 (2002).
[24] C. Virojanadara and L. Johansson, Mater. Sci. Forum **389–393**, 701 (2002).
[25] L. Johansson, C. Virojanadara, T. Eickhoff, and W. Drube, Surf. Sci. **529**, 515 (2003).
[26] J. Pollmann, P. Krüger, M. Rohlfing, M. Sabisch, and D. Vogel, Appl. Surf. Sci. **104**, 1 (1996).
[27] E. Rauls, J. Elsner, R. Gutierrez, and T. Frauenheim, Solid State Commun. **111**, 459 (1999).
[28] E. Rauls, Z. Hanjal, P. Deák, and T. Frauenheim, Mater. Sci. Forum **338–342**, 365 (2000).
[29] E. Rauls, Z. Hajnal, P. Deak, and T. Frauenheim, Phys. Rev. B **64**, 245323 (2001).
[30] Y. Hoshino, S. Matsumoto, K. Ogawa, H. Namba, and Y. Kido, Phys. Rev. B **68**, 073308 (2003).
[31] K. Emtsev, T. Seyller, L. Ley, A. Tadich, L. Broekman, E. Huwald, J. Riley, and R. Leckey, Mater. Sci. Forum **483–485**, 547 (2005).
[32] C. Virojanadara and L. Johansson, Mater. Sci. Forum **483–485**, 581 (2005).
[33] H. Tsuchida, I. Kamata, and K. Izumi, Appl. Phys. Lett. **70**, 3072 (1997).
[34] H. Tsuchida, I. Kamata, and K. Izumi, Jpn. J. Appl. Phys., Part 2 **36**, L699 (1997).
[35] H. Tsuchida, I. Kamata, and K. Izumi, Mater. Sci. Forum **264–268**, 351 (1998).
[36] H. Tsuchida, I. Kamata, and K. Izumi, J. Appl. Phys. **85**, 3569 (1999).
[37] N. Sieber, T. Seyller, B. F. Mantel, J. Ristein, and L. Ley, Mater. Sci. Forum **353–356**, 223 (2001).
[38] N. Sieber, B. F. Mantel, T. Seyller, J. Ristein, and L. Ley, Diamond Relat. Mater. **10**, 1291 (2001).
[39] N. Sieber, B. F. Mantel, T. Seyller, J. Ristein, L. Ley, T. Heller, D. R. Batchelor, and D. Schmeißer, Appl. Phys. Lett. **78**, 1216 (2001).
[40] N. Sieber, T. Seyller, L. Ley, M. Polcik, D. James, J. D. Riley, and R. C. G. Leckey, Mater. Sci. Forum **389–393**, 713 (2002).
[41] N. Sieber, T. Stark, T. Seyller, L. Ley, C. Zorman, and M. Mereghany, Appl. Phys. Lett. **80**, 4726 (2002).
[42] N. Sieber, T. Stark, T. Seyller, L. Ley, C. Zorman, and M. Mereghany, Appl. Phys. Lett. **81**, 1534 (2002).
[43] N. Sieber, T. Seyller, L. Ley, D. James, J. D. Riley, R. C. G. Leckey, and M. Polcik, Phys. Rev. B **67**, 205304 (2003).
[44] T. Seyller, N. Sieber, T. Stark, L. Ley, C. Zorman, and M. Mehregany, Surf. Sci. **532–535**, 698 (2003).
[45] T. Seyller, J. Phys.: Condens. Matter **16**, S1755 (2004).
[46] N. Sieber, T. Seyller, R. Graupner, L. Ley, R. Mikalo, P. Hoffmann, D. R. Batchelor, and D. Schmeißer, Appl. Surf. Sci. **184**, 280 (2001).
[47] N. Sieber, T. Seyller, R. Graupner, L. Ley, R. Mikalo, P. Hoffmann, D. Batchelor, and D. Schmeißer, Mater. Sci. Forum **389–393**, 717 (2002).
[48] S. King, R. Kern, M. Benjamin, J. Barnak, R. Nemanich, and R. Davis, J. Electrochem. Soc. **146**, 3448 (1999).
[49] M. van Hove, W. Weinberg, and C. Chan, *Low-Energy Electron Diffraction* (Springer, New York, 1986).
[50] D. Shirley, Phys. Rev. B **5**, 4079 (1972).
[51] G. Lucovsky, Solid State Commun. **29**, 571 (1978).
[52] E. Aust, G. Dure, M. Groteklaes, K. Schwister, R. Stephan, and P. Volgnandt, *Taschenbuch der Chemie* (Fachbuchverlag Leipzig im Carl Hanser Verlag, 1999).
[53] R. C. Fang and L. Ley, Phys. Rev. B **40**, 3818 (1989).
[54] J. Lander and J. Morrison, J. Appl. Phys. **33**, 2089 (1962).
[55] N. Sieber, M. Hollering, J. Ristein, and L. Ley, Mater. Sci. Forum **338–342**, 391 (2000).
[56] L. I. Johansson, F. Owman, and P. Martensson, Phys. Rev. B **53**, 13793 (1996).
[57] U. Starke, J. Schardt, J. Bernhardt, M. Franke, and K. Heinz, Phys. Rev. Lett. **82**, 2107 (1999).
[58] W. Mönch, *Semiconductor Surfaces and Interfaces Vol. 26 of Springer Series in Surface Science* (Springer, Berlin, 1995).
[59] F. Himpsel, K. Altmann, R. Bennewitz, J. Crain, A. Kirakosian, J.-L. Lin, and J. McChesney, J. Phys.: Condens. Matter **13**, 11097 (2001).